Annual Report, 1999
Analysis of Northridge Aftershocks Amplitude and Damage and Santa Monica High Resolution Experiment

P.M. Davis

Group B

Gao et al. (1996) inferred that focusing was a major factor causing damage in Santa Monica at the time of the Northridge earthquake. Spatial averages of peak amplitudes from the seismograms of the Northridge aftershock array were found to be largest in the damage zone. Alex and Olsen (1997) and Graves et al. (1998) present calculations that suggest other effects may be as or more important, for example shallow site effects, or constructive interference between body and surface waves generated at the basin edge. Furthermore there is significant uncertainty as to the structure of the basin edge which determines where focusing effects are greatest (Graves et al., 1998). The synthetic calculations were 2D and at lower frequencies than the observations where focusing was greatest. We thus test the effects of 3D and frequency on amplification due to focusing.

The peak amplitudes occurred in waves typically of 10 Hz frequency.   Liu (1998) showed that spectral ratios in a high frequency band 8-16 Hz correlated with the amplification patterns determined from measuring peak amplitudes, while for lower bands, the correlation diminished. Thus, the anomalous amplification is a high frequency effect. It remains to be seen whether focusing is the right explanation. The one- and two-story buildings that experienced most of the damage are thought to be susceptible to 0.1 to 0.2 Hz energy. Therefore there is good reason to concentrate on how this band is affected by structures deep beneath Santa Monica.

Geological Focusing

Incident waves refracted at a convex basement-sediment interface will be converted into converging cylindrical or spherical waves of limited aperture, determined by the extent of the structure and the wavelengths involved. The equations of optical focusing (Marcuse, 1973; Born and Wolfe, 1970) can be used to describe these dependencies.

In the Debye approximation (i.e., neglecting diffracted edge effects), the diffracted field in the focal plane of a converging cylindrical wave of initial amplitude A is,

$$w(x) = \frac{2LA}{\sqrt{lf}} \sin c(v) \qquad (1)$$

$$v = \frac{2pLx}{fl}$$

where ±L is the aperture, f is the focal distance, λ the wavelength, x is the distance from the focus, and the asymptotic limit is assumed i.e., λ<<f. For the three-dimensional case the amplitude of a diffracted converging spherical wave is given by

$$w(r) = \frac{pL^2}{lf} 2J_1(v)/v \qquad (2)$$

The amplification in the three-dimensional case is approximately the amplification of the two-dimensional case squared, other parameters being equal. Two-dimensional calculations therefore underestimate three-dimensional focusing.

Finite Difference Calculations

We have carried out high frequency SH finite difference calculations of seismic propagation through models having slightly modified sub-basin cross-sections from those presented by Wright (1991). These models exhibit localized amplification by a factor of 6, highly dependent on radii of curvature, wavelength and velocity contrast. An example is shown in figure 1 where a curved interface separates bedrock of S-wave velocity V_s= 3.2 km/s from sediments of V_s=1.6 km/s. We found that the amplifications achieved in the FD calculation in figure 1 agree with equation (1) over a wide range of frequencies. Therefore we judge that it is valid to use equation (2) to estimate the three-dimensional effects and as a simple forward model to invert focusing effects.

Data Analysis

Gao et al. (1996) showed that spatially averaged ratios over the region of damage (so called S ratios) were higher than similarly constructed ratios in undamaged regions. However this spatial averaging did not take into account the spatial variability within the damage zone. In last year's report we tested a model where the amplitude fall-off of focusing was assumed to be Gaussian. We now use the Bessel function fall-off given by equation (2). That model fits the concentrations of damage in the NW quadrant of the damage zone but leaves high amplitudes in other areas un-modeled. An excellent fit was found with a lens at a depth of 2.1 km and radius of curvature 1km, with a velocity contrast given by the SCEC velocity model. The lens location fits very close to where Wright‘s (1996) KK' cross-section shows the reverse-dipping Santa Monica fault intersecting the basement. Rays were traced from the aftershock hypocenter to the assumed hemi-spherical interface and then to the surface (Figure 2) where equation (2) was used to describe the spatial fall-off. The data were divided by coda amplitudes to minimize site effects. An inversion of the site-corrected data gave excellent statistical results.

In order to model remaining areas within the damage zone not covered by the original lens, we added new lenses and applied the F-test to determine which were significant. The basic assumption was that the basin edge concentrates energy, but in patches of bright constructive interference and dark destructive interference. The bright patches could be modeled as converging spherical waves generated at undulations of the basement sediment-interface. We fit a total of 7 such lenses, but only 5 survived the F-test. Figure (3a,3b) shows color-contoured amplitudes of the data, side by side with the theoretical amplitudes of the multi-lens model. The fit is excellent and explains 89% of the variance. In the second to last panel of figure 3 we plot the coda factors. There it is seen that site effects, as judged by relative coda amplitudes, can account for a factor of 2 as one crosses the Santa Monica fault, but the other panels show that constructive interference can be larger adding a factor of 3 or more.

In the bottom right panel of figure 3 we have constructed a synthetic Northridge earthquake amplification field by using the fault patches of Zeng and Anderson (1996) as sources, and tracing rays through the lens structure. Also plotted are the red-tagged buildings (in white). The match between expected amplification and red-tagged distribution is satisfactory, given there were no stations in the east where the energy appears low.

Figure 1. Finite difference simulations for a 2D Ricker wavelet passing through a hemi-cylindrical interface (top left). Each panel is a snapshot at various times. This model gives good agreement with equation (1).

Figure 2. Ray tracing to an assumed hemispherical lens from each of 22 aftershocks used by Gao et al., to infer focusing in Santa Monica. A Bessel falloff with distance (equation 2) is used to model the spatial distribution at the surface. Multiple lenses such as this are used to construct a composite interference field to explain the aftershock data.

Figure 3a: Santa Monica aftershock survey amplitudes. Each pair of color images corresponds to
the measured and theoretical amplitudes from a Northridge aftershock. Those on the left hand side
are measured amplitudes, while those on the right give the theoretical images. The model consists of a 5 hemispherical lenses at a depth of about 2 km north of the Santa Monica Fault (depicted by the ENE line). The lower left line corresponds to the coastline.

Figure 3b: A in Figure 3a. Second to last panel plots coda amplitudes. Bottom right is amplification from a model of the Northridge earthquake passing through the lens structures. White dots give locations of red-tagged buildings.

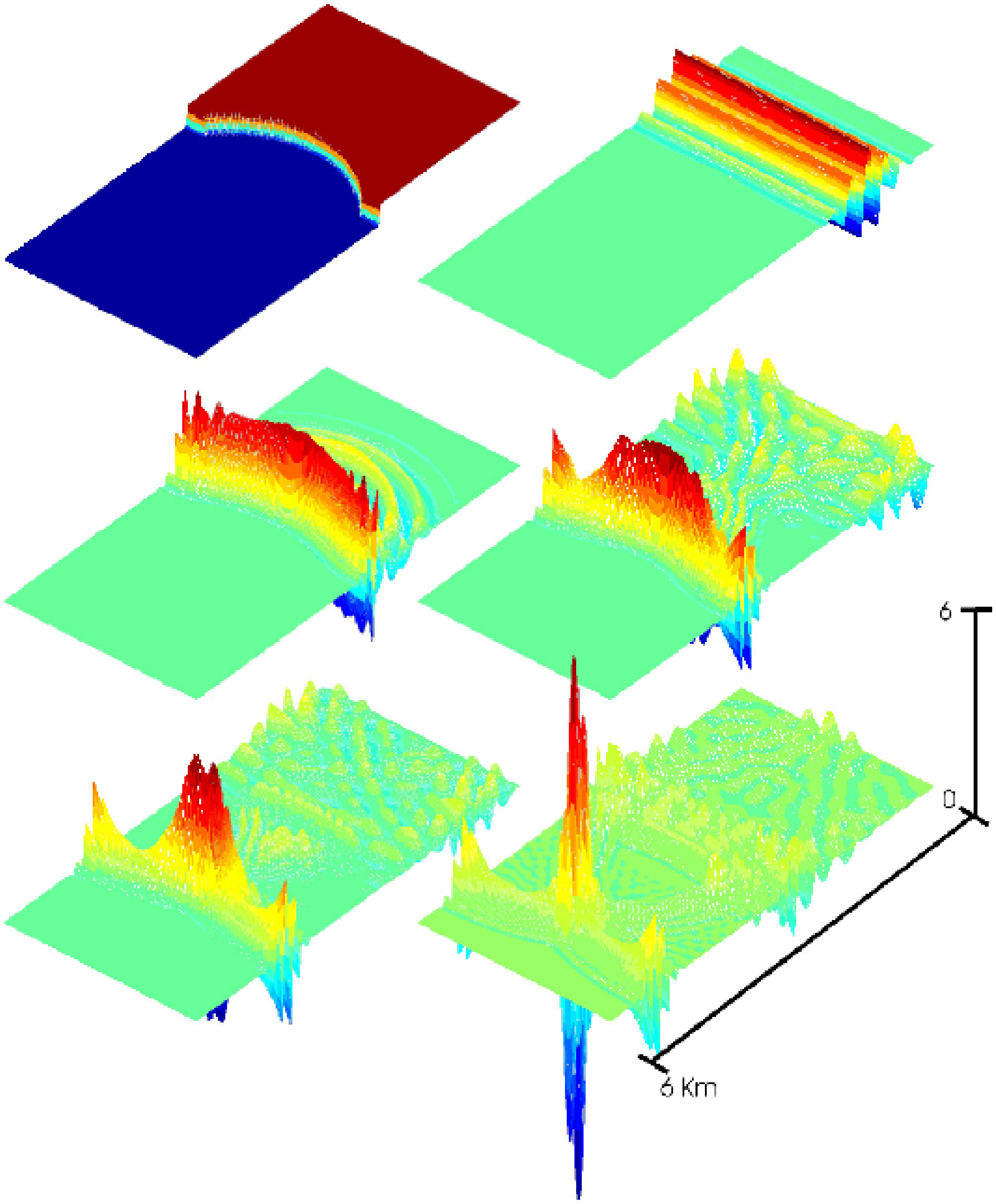
6
0
6 Km

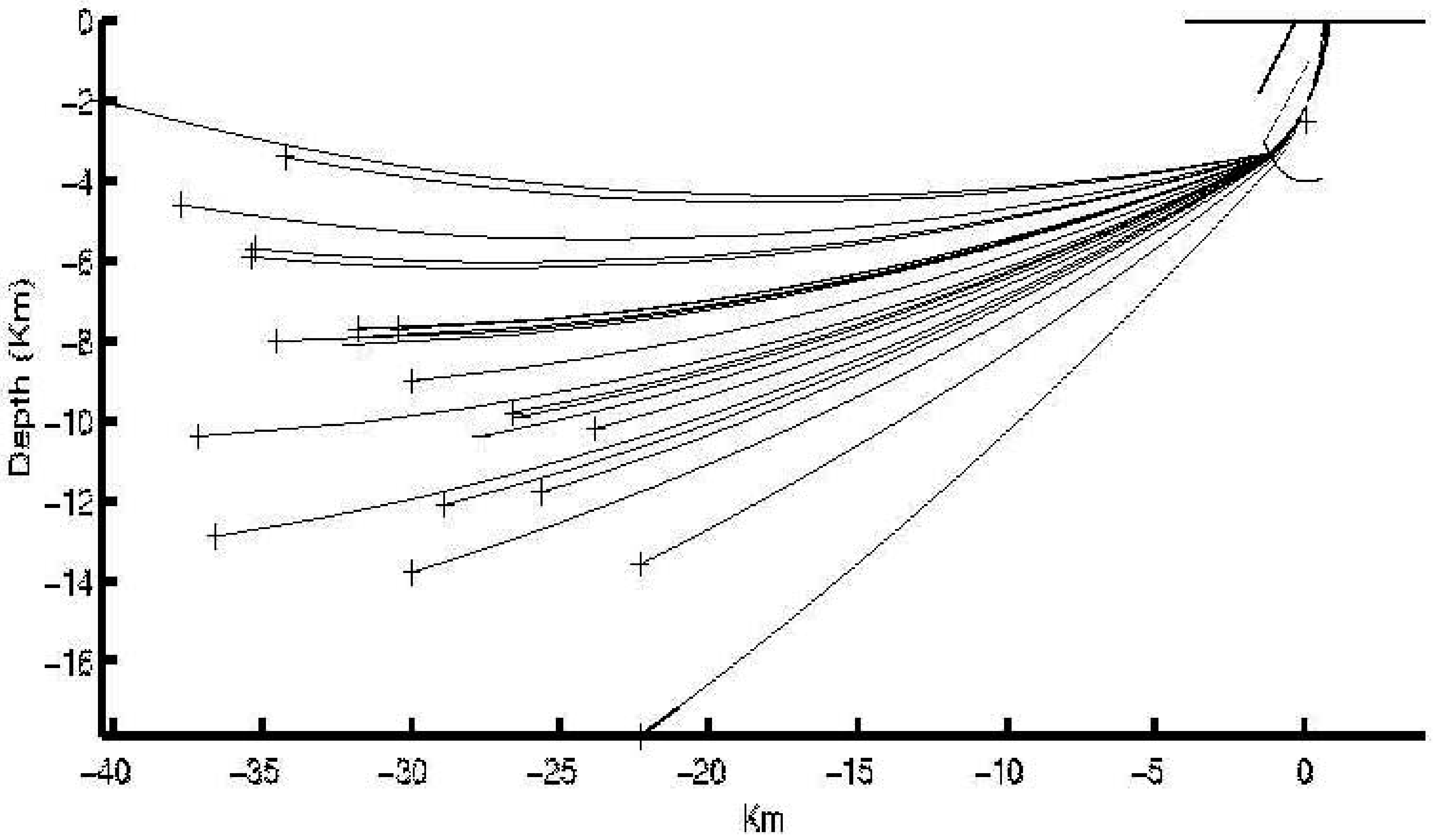

0
-2
-4
-6
-8
-10
-12
-14
-16
Depth (Km)
-40
-35
-30
-25
-20
-15
-10
-5
0
Km

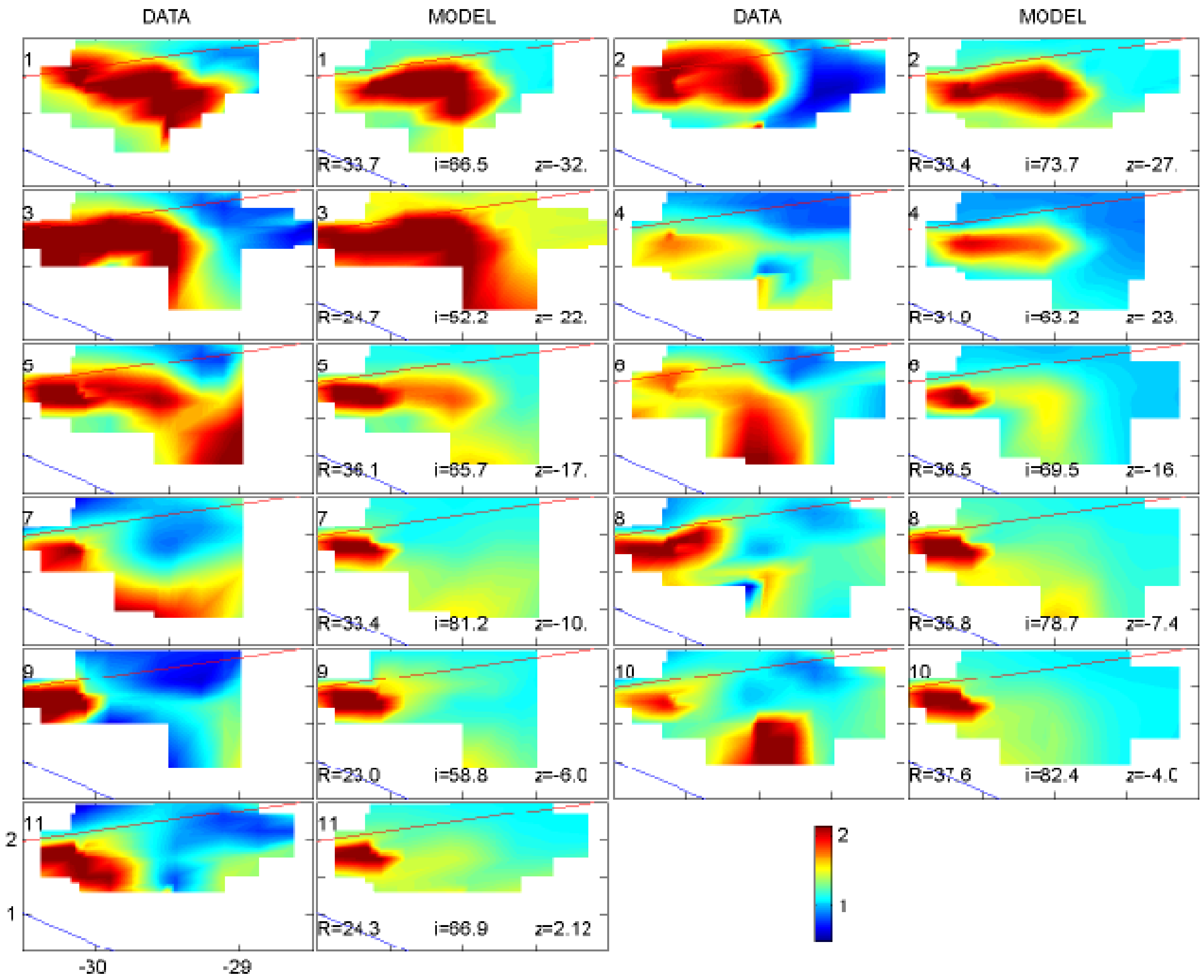
DATA
MODEL
DATA
MODEL
1
1
R=33.7 i=66.5 z=-32.
2
2
R=33.4 i=73.7 z=-27.
3
3
R=24.7 i=62.2 z= 22.
4
4
R=31.0 i=63.2 z= 23.
5
5
R=36.1 i=65.7 z=-17.
6
6
R=36.5 i=69.5 z=-16.
7
7
R=33.4 i=81.2 z=-10.
8
8
R=36.8 i=78.7 z=-7.4
9
9
R=23.0 i=58.8 z=-6.0
10
10
R=37.6 i=82.4 z=-4.0
11
11
R=24.3 i=66.9 z=2.12
2
1
-30
-29
2
1

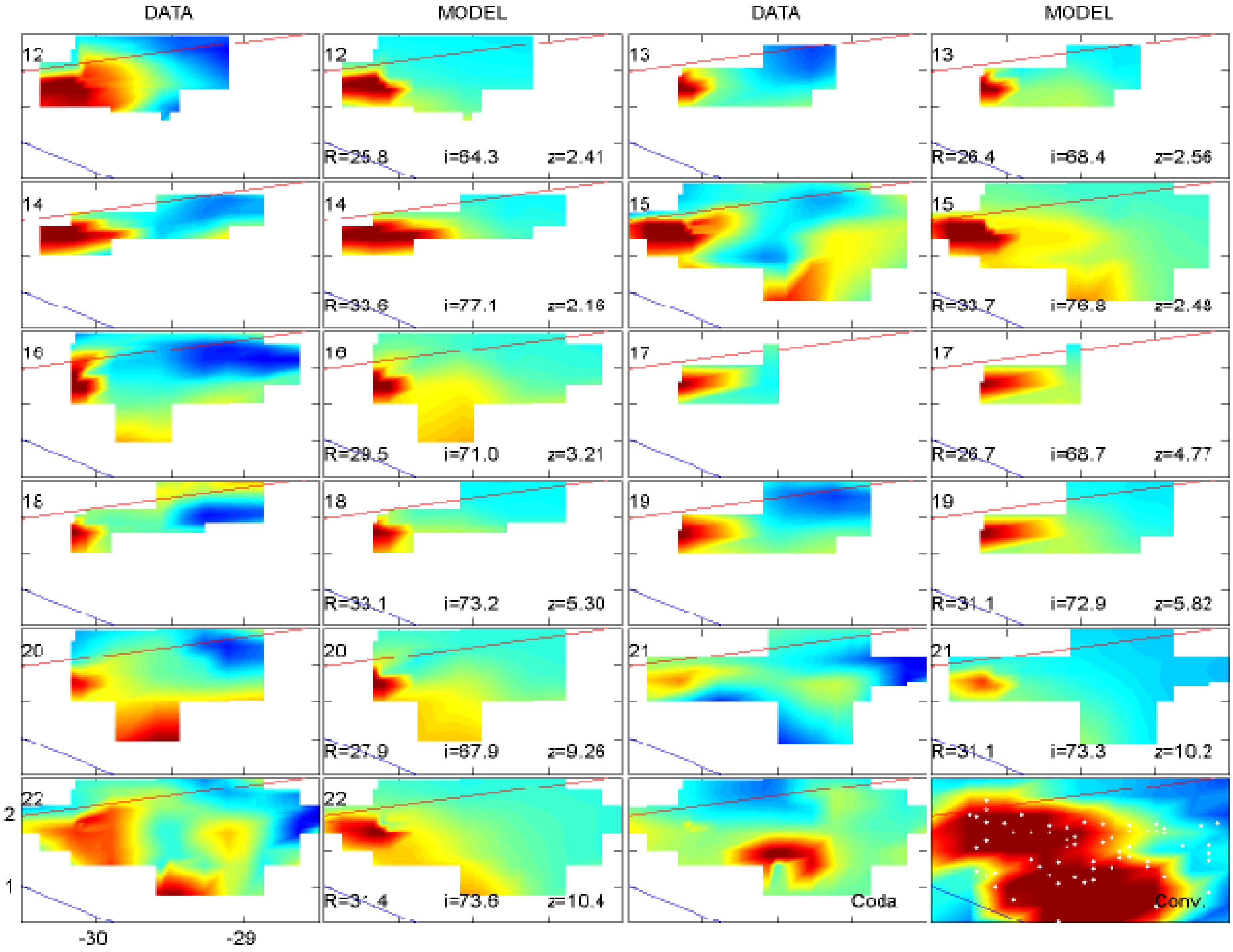
DATA
MODEL
DATA
MODEL
12
12
R=25.8
i=64.3
z=2.41
13
13
R=26.4
i=68.4
z=2.56
14
14
R=33.6
i=77.1
z=2.16
15
15
R=33.7
i=76.8
z=2.48
16
16
R=29.5
i=71.0
z=3.21
17
17
R=26.7
i=68.7
z=4.77
18
18
R=33.1
i=73.2
z=5.30
19
19
R=31.1
i=72.9
z=5.82
20
20
R=27.9
i=67.9
z=9.26
21
21
R=31.1
i=73.3
z=10.2
22
22
R=31.4
i=73.6
z=10.4
Coda
Conv.
2
1
-30
-29